Quantification of transport and binding parameters using Fluorescence Recovery After Photobleaching

Potential for in vivo applications

Eric N. Kaufman and Rakesh K. Jain
Department of Chemical Engineering, Carnegie Mellon University, Pittsburgh, Pennsylvania 15213-3890 USA

ABSTRACT Fluorescence Recovery After Photobleaching (FRAP) has been used extensively in the study of transport and binding in biological media in vitro. The present study adapts and further develops FRAP so that it may be utilized for the in vivo quantification of binding parameters. The technique is validated in vitro by measuring mass transport and binding parameters for the Concanavalin A/Mannose binding system (a diffusion-limited system). The pseudo-equilibrium constant (the product of the equilibrium constant and the total concentration of binding sites) for this system was determined to be 26 ± 15 which compares favorably with literature values ranging between 16 and 32. The applicability of this technique to measure parameters for monoclonal antibody/antigen interactions in a thin tissue preparation such as the rabbit ear chamber tissue preparation is also examined. Unlike other methods for measuring binding parameters, this is the only technique which has the potential to measure parameters relevant to antibody delivery in vivo. The proposed technique is noninvasive and does not require a priori knowledge of, independent measurement of, or variation in the concentration of binding sites or total concentration of binding species.

INTRODUCTION

Monoclonal antibodies and other novel products of genetic engineering have not realized their promise in the treatment of solid tumors to date due to their poor delivery to tumors (1). The delivery and distribution of any agent in a tissue is governed by mass transport and binding parameters. While measurements of mass transport parameters have been made in vivo, there are no in vivo measurements of binding parameters to date. Binding parameters measured in single cells (2), or multicellular spheroids (3) grown in vitro, while useful, may not be representative of the in vivo situation. The use of Fluorescence Recovery After Photobleaching in conjugation with the rabbit ear chamber (4, 5) or similar tissue preparation offers the ability, for the first time, to quantify mass transport and binding parameters noninvasively in normal and tumor tissues in vivo. This technique has the potential to provide clinically relevant parameters which may be used to predict monoclonal antibody distribution in vivo.

To date, photobleaching methods have been developed to study the lateral diffusion and binding of membrane proteins in vitro. Using Total Internal Reflection Microscopy and Fluorescence Photobleaching Recovery (TIR/FPR) residence times of bovine serum albumin on fused silica (6), binding parameters for IgG and insulin on albumin-coated silica (7) and binding parameters for epidermal growth factor on erythrocyte ghost membranes (8) have been reported. While quite successful in in vitro applications, these techniques are designed for the study of two-dimensional surface kinetics and therefore have not been applied to the task of measuring diffusion and binding in an in vivo tissue preparation.

Various models of binding have been proposed to measure parameters during photobleaching or concentration jump experiments, yet none are easily applied to in vivo experiments. Elson and Reidler (9) propose a model that may be used for diffusion-limited systems. They extract the equilibrium constant by measuring the effective diffusion coefficient as a function of the concentration of binding sites. This is impractical in vivo where not all reactions are diffusion limited. The paper's suggestion that the length scale of the photobleach could be increased to make any system diffusion limited is impractical in vivo where the length scale of the bleach is limited by the proximity of blood vessels which would contribute significant error if they were to lay in the photobleached area. Furthermore, in vivo the concentration of sites may not be known a priori, and only rarely can the concentration of sites be modified. Koppel (10) presents a method to obtain binding kinetics using periodic pattern photobleaching. While this method is not restricted to the diffusion or reaction limits, one must vary the periodicity of the pattern to achieve closure. This method has not been applied in vivo to date due to the difficulty in obtaining periodic pattern photobleaches in an in vivo system.

Please address reprint requests to Dr. Jain.

Fluorescence Recovery After Photobleaching (FRAP) using Gaussian point-wise video digitization (GPD) was proposed by Chary and Jain (11) as a means of measuring convective velocity fields without a priori knowledge of the direction of flow. This technique has been calibrated in vitro (12) and has been used in vivo to quantify diffusion coefficients of serum-soluble proteins and convective velocity fields in normal and neoplastic tissue (5) through the use of a rabbit ear chamber (4). In FRAP with GPD, a Gaussian profile is photobleached onto the region of interest. Rather than using a photodiode which detects light from the entire image, the image is point-wise digitized to obtain the fluorescence intensity at each picture element (pixel) in the region. The intensity profile as a function of radial position is fit to a Gaussian function at each time point to accurately track the center point intensity and position of the bleach. Through minimization of the sum of squares error between the predicted and measured center point intensity, mass transport parameters can be obtained. In this paper, we develop models for the in vivo application of GPD in measuring mass transport and binding parameters, assess the accuracy of this technique in vitro, and discuss its possible in vivo applications. FRAP in conjunction with a thin transparent tissue preparation seems to have the potential to allow clinically relevant determination of antibody/antigen kinetics.

THEORETICAL STUDY

Model development

One of the simplest models of binding is the case of reversible binding to one type of site. Such would be the case for a monoclonal antibody or Concanavalin A (Con A) molecule which does not exhibit nonspecific binding or entrapment. This model has proven to be effective in both monoclonal antibody and Con A studies (13, 14) and is an excellent approximation if the molecule does bind to more than one type of site if secondary sites form unstable complexes or are sparse. The feasibility and sensitivity of using FRAP with GPD to quantify mass transport and binding parameters both in vivo and in vitro are assessed by solving the diffusion equation for this binding system.

The diffusion equation with reversible binding to one type of site assuming uniform distribution of binding sites, an immobile bound complex, and no convective field is:

$$C_{1i} + Ag \underset{k_{-1}}{\overset{k_1}{\rightleftharpoons}} C_{2i} \tag{1}$$

$$\frac{\partial C_{1i}}{\partial t} = D\nabla^2 C_{1i} - k_1 C_{1i} Ag + k_{-1} C_{2i} \tag{2}$$

$$\frac{\partial C_{2i}}{\partial t} = k_1 C_{1i} Ag - k_{-1} C_{2i}. \tag{3}$$

These equations must be written for both fluorescently active ($i = a$) and bleached ($i = b$) macromolecules.

C_{1i} = concentration of mobile macromolecule.

C_{2i} = concentration of immobile (bound) macromolecule.

Ag = concentration of vacant binding sites.

The geometry of the system is cylindrical with dependence only in the radial direction (r)[1] so that:

$$\nabla^2 C = \frac{1}{r}\frac{\partial}{\partial r}\left(r\frac{\partial C}{\partial r}\right). \tag{4}$$

The initial condition is imposed by the Gaussian intensity profile of the laser beam[2] and by the facts that the bound and unbound components are in equilibrium and are bleached to the same extent:

$$C_{Ta}(r, t = 0) = C_{TB} + (C_{TU} - C_{TB})\left[1 - \exp\left(\frac{-2r^2}{R_0^2}\right)\right] \tag{5}$$

$$\frac{k_1}{k_{-1}} = \frac{C_{2a}}{C_{1a}\,Ag} = \frac{C_{2a}}{C_{1a}(Ag_0 - C_{2a} - C_{2b})} \tag{6}$$

$$\frac{k_1}{k_{-1}} = \frac{C_{2b}}{C_{1b}\,Ag} = \frac{C_{2b}}{C_{1b}(Ag_0 - C_{2a} - C_{2b})}. \tag{7}$$

C_{Ti} = total concentration of macromolecule = $C_{1i} + C_{2i}$ (C_{Ta} is measured).

C_{TU} = total concentration of fluorescently active macromolecule well beyond the bleached region.

C_{TB} = total concentration of fluorescently active macromolecules at $r = 0$ and $t = 0$.

R_0 = radius of the bleached spot at $t = 0$ such that $C_T(R_0, t = 0) = (1 - 1/e^2)C_{TU}$, i.e., the Gaussian radius of the bleach.

Ag_0 = total concentration of binding sites.

C_{TU}, C_{TB}, and R_0 are obtained by fitting the data to a Gaussian function. The initial conditions and definition of C_{TA} represent four nonlinear algebraic equations for the

[1]The characteristics of our bleaching beam have been described previously (12). The diameter of the beam (d) entering the objective is 494 μm and the focal length (f) of our 20× objective is 8 mm. Using the formula (48):

$$DOF = \frac{8\lambda}{\pi}\left(\frac{f}{d}\right)^2$$

yields a depth of focus (DOF) of 325 μm, several times the depth of our preparation.

[2]Eq. 5 is valid only for "shallow" bleaches (11). Axelrod (49) presents formulations incorporating arbitrary extents of photobleaching.

initial concentrations of the four components. These equations were solved numerically.

The boundary conditions are:

$$\nabla C_{1i} = \nabla C_{2i} = 0 \quad \text{at } r = 0 \quad \text{and as } r \rightarrow \infty. \tag{8}$$

The equations were made dimensionless by introducing the following groups:

$$\theta_{Ta} = \theta_{1a} + \theta_{2a} = \frac{C_{Ta} - C_{TB}}{C_{TU} - C_{TB}}$$

$$\theta_{1a} = \frac{C_{1a}}{C_{TU} - C_{TB}} \quad \theta_{2a} = \frac{C_{2a} - C_{TB}}{C_{TU} - C_{TB}} \tag{9}$$

$$\theta_{Tb} = 1 - \theta_{Ta} = \theta_{1b} + \theta_{2b} = \frac{C_{Tb}}{C_{TU} - C_{TB}}$$

$$\theta_{1b} = \frac{C_{1b}}{C_{TU} - C_{TB}} \quad \theta_{2b} = \frac{C_{2b}}{C_{TU} - C_{TB}} \tag{10}$$

$$z = \frac{r}{R_0} \quad \tau = \frac{Dt}{R_0^2} \quad Da = \frac{R_0^2 k_1 A g_0}{D}$$

$$\alpha = \frac{C_{TB}}{Ag_0} \quad \beta = \frac{k_1 A g_0}{k_{-1}} \quad \gamma = \frac{C_{TB}}{C_{TU} - C_{TB}}. \tag{11}$$

As a result, the equations describing the fluorescence recovery after photobleaching become:

$$\frac{\partial \theta_{1a}}{\partial \tau} = \frac{1}{z}\frac{\partial}{\partial z}\left(z\frac{\partial \theta_{1a}}{\partial z}\right) - Da\left\{\theta_{1a}\left[1 - \alpha\left(\frac{\theta_{2a} + \theta_{2b}}{\gamma} + 1\right)\right] - \frac{\theta_{2a} + \gamma}{\beta}\right\} \tag{12}$$

$$\frac{\partial \theta_{2a}}{\partial \tau} = Da\left\{\theta_{1a}\left[1 - \alpha\left(\frac{\theta_{2a} + \theta_{2B}}{\gamma} + 1\right)\right] - \frac{\theta_{2a} + \gamma}{\beta}\right\} \tag{13}$$

$$\frac{\partial \theta_{1b}}{\partial \tau} = \frac{1}{z}\frac{\partial}{\partial z}\left(z\frac{\partial \theta_{1b}}{\partial z}\right) - Da\left\{\theta_{1b}\left[1 - \alpha\left(\frac{\theta_{2a} + \theta_{2b}}{\gamma} + 1\right)\right] - \frac{\theta_{2b}}{\beta}\right\} \tag{14}$$

$$\frac{\partial \theta_{2b}}{\partial \tau} = Da\left\{\theta_{1b}\left[1 - \alpha\left(\frac{\theta_{2a} + \theta_{2b}}{\gamma} + 1\right)\right] - \frac{\theta_{2b}}{\beta}\right\}, \tag{15}$$

where θ_{Ta} is the dimensionless total concentration of fluorescently active macromolecule (reported as θ on the accompanying figures) and θ_{1i} and θ_{2i} represent the mobile and immobile components, respectively. Z is the dimensionless radial coordinate and τ the dimensionless time. Da, α, β, and γ represent the Damkoehler number (the system is diffusion limited when $Da \gg 1$ and reaction limited when $Da \ll 1$), extent of saturation, pseudo-equilibrium constant, and depth of bleach. The four coupled nonlinear partial differential equations were solved numerically.

Assessment of numerical solution

Analytical solutions to the above non-linear equations exist when (*a*) no binding occurs (5) or (*b*) binding is instantaneous ($Da \gg 1$ and $\alpha \ll 1$). In an instantaneous reaction (diffusion limited), the bleached and active components are always in equilibrium. Crank (15) demonstrates that for such a case the solution is identical to that of the nonbinding case except that the diffusion coefficient is reduced by a factor of $1 + \beta$. Thus the analytical solutions for the dimensionless center point concentration as a function of dimensionless time are:

$$\theta_{Ta}(z = 0, \tau) = \frac{8\tau}{1 + 8\tau}$$

$$\text{and} \quad \theta_{Ta}(z = 0, \tau) = \frac{\frac{8}{\beta + 1}\tau}{1 + \frac{8}{\beta + 1}\tau} \tag{16}$$

for no binding and instantaneous binding, respectively. Comparison of the numerical to the analytical solution for the above two cases shows excellent agreement between the solutions (data not shown).

Sensitivity of gaussian point-wise digitization

As discussed previously, the GPD technique monitors the fluorescence intensity at the center of the bleach as a function of time to obtain the mass transport and reaction parameters. Previous experiments (5) have measured diffusion coefficients in vivo using this technique with an accuracy of at least ±50%. For the presence of binding to be detected by FRAP in vivo, binding must slow the recovery to an extent greater than a 50% reduction in the diffusion coefficient. FRAP is feasible for a binding system if the recovery curve does not intersect the shaded area of Figs. 1, 3, 6, 10 *a*, and 10 *b* which represents the error associated in measuring D for the nonbinding case.

In measuring the mass transport parameters for a given interaction, one could possibly control the parameters C_{TU}, D, R_0, Ag_0, and γ. As seen in Fig. 1, when C_{TU} is greater than Ag_0, the fluorescence recovery curve is no different from that of diffusion alone. This is due to the fact that the binding sites are saturated and mobile species are able to diffuse unhindered by the effects of binding. FRAP will not be able to obtain meaningful binding parameters in this case due to the fact that a model of diffusion only would fit the data with equal ability as a binding model. When C_{TU} is less than Ag_0, recovery occurs mainly through the dissociation of the bound complex because there are very few free molecules.

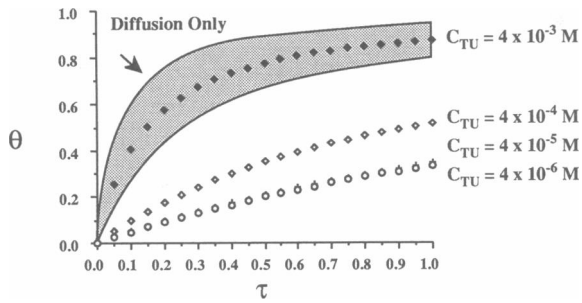

FIGURE 1 Dimensionless concentration of fluorescently active macromolecule at the center point as a function of dimensionless time and concentration of binding species. The shaded region represents the area in which recovery is not significantly different from that of diffusion alone and binding parameters cannot be obtained. Parameters used for this simulation are: $Da = 1{,}646$, $\beta = 15$, $\gamma = 3$, and $Ag_0 = 6 \times 10^{-4}$ M. FRAP will discern the recovery with binding from that of diffusion alone when the concentration of binding species is less than the concentration of binding sites.

In this case, recovery is significantly different from that of diffusion alone and application of FRAP/GPD should yield the parameter β if the system is instantaneous, or the parameters k_1, k_l, Ag_0, and D (through numerical solution of Eqs. 12–15) if the binding regime is noninstantaneous (reaction limited). When Eqs. 12–15 are rearranged to obtain θ as a function of real time rather than dimensionless time, R_0 and D do not appear in any of the binding terms. Thus, while decreasing D or increasing R_0 will cause the recovery to occur more slowly, it will not dissociate the recovery with binding from that of diffusion alone. Altering the extent of the bleach γ while keeping C_{TU} constant, accomplished experimentally by altering the laser exposure time, does not affect the recovery because it does not alter the kinetics of the interaction.

EXPERIMENTAL STUDY

One of the most widely studied biological binding interaction is that of the lectin Con A with gluco and manno sugar residues (14, 16–18). The present study measures the mass transport and reaction parameters for Con A's interaction with Mannose in vitro using FRAP with GPD and compares these values to those previously published using other measurement techniques to assess the accuracy of the proposed technique. This study demonstrates that FRAP/GPD is capable of reproducing mass transport and reaction parameters for Concanavalin A and shows promise as a tool for quantifying these parameters for monoclonal antibody/antigen interactions for the first time in vivo.

Samples

Fluorescein Isothiocyanate labeled succinyl-Concanavalin A (FITC-suc-Con A) was obtained from Sigma Chemical Co. (Product #L-9385, Lot #118F8055; St. Louis, MO). Succinylation ensures that the species exists as a dimer of molecular weight 56,000 g/mol (19). The dye to protein ratio of the lot used was 1.3. Experiments to measure the free diffusion coefficient of FITC-suc-Con A prepared a 1×10^{-5} M solution of the species in 0.5 M NaCl. All samples were drawn by capillary action into a 50-μm thick glass capillary slide (#W5005; Vitro Dynamics, Rockaway, NJ) for observation conducted at 23 ± 2°C. Experiments to measure the diffusion coefficient of Con A with binding to Mannose required that the binding sites be uniformly distributed and immobilized. To achieve this, Mannose covalently bound to sepharose beads which themselves are inert to Con A (Product #M 6400, Lot #67 F-9591; Sigma Chemical Co.) was homogenized by continuous stirring for 72 h. Sigma Chemical Co. estimates the concentration of immobilized Mannose on product #M 6400 to be between 6.5×10^{-4} and 1.3×10^{-3} M. These beads are supplied in 0.5 M NaCl. In preparing the sample for the binding experiments, homogenized Mannose-sepharose and 3.8×10^{-6} M FITC-suc-Con A in 0.5 M NaCl were mixed 1:1 and drawn into the 50-μm capillary slide for observation. Two types of samples were used to measure the diffusion coefficient of FITC-suc-Con A in a sepharose matrix with no binding. The first sample was a 1:1 mixture of 3.8×10^{-6} M FITC-suc-Con A and homogenized sepharose beads that did not contain Mannose (Product #CL 4B200 Lot #58 F-0376, Sigma Chemical Co.). The second sample consisted of a saturating concentration of Con A (4×10^{-3} M) in the same Mannose-sepharose used in the binding experiments. Saturating conditions ensured that the effect of binding was negligible (Fig. 1) and the use of the Mannose-sepharose matrix ensured equal tortuosities in binding and nonbinding preparations. There was no statistical difference ($p = 0.14$) between the two nonbinding samples.

Equipment

The equipment, experimental procedure, and data analysis technique used in this study are nearly identical to those described in reference (12). Briefly, the capillary slide was trans-illuminated at 480 nm by a mercury vapor lamp (model HBO 100W; Zeiss, Morgan Instruments, Cincinnati, OH). Light passed through a heat reflector (model Califax; Carl Zeiss, Inc., Thornwood, NY), heat absorber (model KG-1; Carl Zeiss, Inc.), FITC exciter, and red absorber filters (models 46-79-79 and 46-78-85; Carl Zeiss, Inc.). The microscope was focused on the

sample using a 20× objective (model F-LD 20/0.25, 46-06-05; Carl Zeiss, Inc.). Light emitted from the sample was passed through a barrier filter (model 46-78-33; Carl Zeiss, Inc.) and the 1.25× lens in a Zeiss Optovar (model 47-16-45; Carl Zeiss, Inc.) installed in the microscope barrel. The image was monitored using a Silicon Intensified Target camera (model 4400; Cohu, Inc., San Diego, CA) operated in a range where measured intensity was linear with fluorophore concentration (20), and the signal sent to an image analysis system (DT-IRIS; Data Translation, Marlboro, MA) housed in an IBM PC-AT allowing on-line digital analysis of the video image.

A 5-W argon ion laser (488 nm) (model 2000-5; Spectra Physics, Mountain View, CA) was used to photobleach the sample. The laser beam was directed through a spatial filter (model 910B; Newport Corporation, Fountain Valley, CA) and focused using a 5× microscope objective (model M-5X, Newport Corporation). The beam accessed the sample via the epi-illumination port where it was attenuated using neutral density filters (models 46-78-40, -41, -42; Carl Zeiss, Inc.). Two shutters (Uniblitz Electronic, Vincent Assoc., Rochester, NY) were used to control the bleaching time and light reaching the camera. The shutters were electronically controlled, allowing a bleach time as low as 10 ms.

Experimental procedure

After background image acquisition and storage, a region in the sample was photobleached for 0.01–0.2 s (depending upon the preparation). Upon closing the laser shutter, the camera shutter was opened to allow imaging of the sample. As described in reference 12, five frames were averaged at every time point to ensure an acceptable signal-to-noise ratio. The process of acquiring and storing the frames took ~1.4 s for each time point. The data from the monitoring region (90 × 70 pixels or less) was stored in the system buffers. This process was continued for up to 15 s after the bleach. After the background image was subtracted, the data were stored for subsequent analysis.

Analysis procedure

Data analysis was conducted on a Sun Microsystems, Inc. (Mountain View, CA) 3/260 workstation. A gaussian profile was fit to the intensity data at each time point using nonlinear parameter estimation (21). This fitting enabled accurate tracking of the center point fluorescence intensity. Mass transport and binding parameters were obtained by minimizing the sum of squares error between the model (Eq. 16) and the measured center point concentrations.

RESULTS

Because the Damkoehler number for the binding of Con A to Mannose is much greater than unity (17, 22) the instantaneous binding model (Eq. 16) was used for this in vitro calibration. Assessment of accuracy was based on the comparison of the pseudo-equilibrium constant β obtained by our technique to the literature value of β obtained by other methods. To establish a baseline, the free diffusion coefficient (D_0) of FITC-suc-Con A was measured. The diffusion coefficient of this same species in a nonbinding system (D) is $<D_0$ due to the tortuosity of the sepharose matrix. The diffusion coefficient in a binding system (D_{eff}) is reduced due to both tortuosity and the immobilization reaction. β was obtained by rearranging Eq. 16 to yield:

$$\beta = \frac{D}{D_{\text{eff}}} - 1. \tag{17}$$

Gaussian fits of the fluorescence intensity as functions of radial position and time as well as comparison between measured and predicted center point concentration as a function of time for nonbinding and binding experiments are shown in Fig. 2. Results of the in vitro calibration are shown in Table 1.

DISCUSSION

FRAP/GPD is capable of accurately and noninvasively quantifying the pertinent transport and binding parameters for a given binding regime from a single photobleach, without previous knowledge of system parameters. This technique will allow for the first quantification of binding parameters in vivo. The one site model assumes a uniform distribution of binding sites and neglects secondary binding, thermal effects, and convection. The implications of these assumptions to both in vitro and in vivo experiments are discussed and the problem of paucity of data in determining the parameters of interest is addressed.

IN VITRO APPLICATIONS

Experimental calibration

The free diffusion coefficient measured for dimeric Con A agrees favorably with that predicted by the Stokes-Einstein equation for a prolate ellipsoid (23) with succinyl-Con A's dimensions (24) and is slightly higher than that measured for trimeric Con A (molecular weight 84,000) (22) as expected. Sigma Chemical Co. estimates the concentration of Mannose on product M-6400 to be

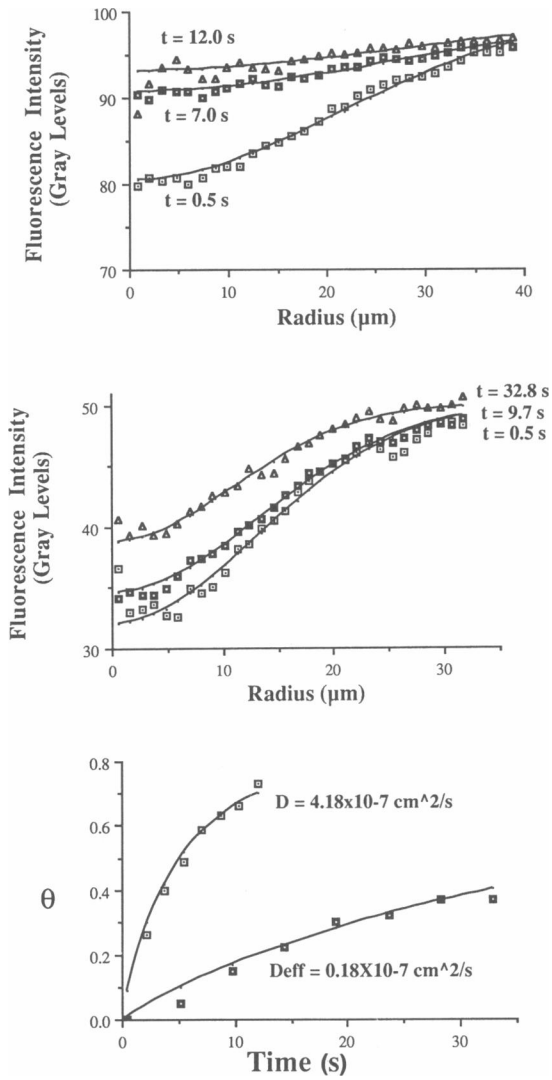

FIGURE 2 Fluorescence intensity as a function of radial position was fit to a gaussian function at each time point to accurately track the center point concentration. The data were fit to a gaussian function using each of the 6,300 pixel values in the monitoring region. Data points have been condensed in Fig. 2, *a* and *b* for the sake of clarity. Fig. 2, *a* and *b* are representative curves from nonbinding and binding bleaches, respectively. The center point intensity as a function of time is used to determine the diffusion coefficient as shown in Fig. 2 *c* . The standard deviations of the center point concentrations are <0.007 and cannot be seen. These bleaches yielded diffusion coefficients of $4.18 \pm 0.26 \times 10^{-7}$ cm^2/s and $0.18 \pm 0.02 \times 10^{-7}$ cm^2/s for nonbinding and binding systems, respectively.

between 6.5×10^{-4} and 1.3×10^{-3} M. Farina and Wilkins (17) report the equilibrium constant for the Con A/Mannose interaction to be 2.5×10^4 M^{-1}, yielding a value of β between 16 and 32. Using FRAP/GPD, β was determined to be 26 ± 15, in good agreement with Farina's value. The large standard deviation associated in

TABLE 1

D_0		$7.4 \pm 1.6 \times 10^{-7}$ cm^2/s	($n = 60$)
D		$3.8 \pm 0.81 \times 10^{-7}$ cm^2/s	($n = 39$)
D_{eff}		$0.14 \pm 0.05 \times 10^{-7}$ cm^2/s	($n = 40$)
		Measured	Literature
	β	26 ± 15	16–32

D_0 = free diffusion coefficient, D = diffusion coefficient in nonbinding system, D_{eff} = effective diffusion coefficient in sepharose matrix with binding to Mannose, β = pseudo-equilibrium constant for the binding interaction. Values are reported as mean ± SD. Parameters measured by FRAP are in good agreement with literature values.

reporting β is due to the fact that because β is obtained by taking the ratio of two variables each having associated error, the relative error in β is the sum of the relative errors of D and D_{eff}.

Model assumptions

Uniform distribution of binding sites

The one site model assumes than the binding sites are uniformly distributed throughout the region of interest. In the Con A/Mannose binding experiments, 60–140-μm diam sepharose beads were homogenized by continuous stirring for 72 h resulting in pieces that were <5 μm in largest dimension. Due to the fact that any inhomogeneity is averaged vertically over the 50-μm thickness of the capillary tube and horizontally over the ~45-μm radius of the photobleach, the continuum hypothesis may be used. If inhomogeneity were a problem, it would be evidenced in a bimodal distribution of diffusion coefficients. Diffusion coefficients would be low when the bleached region was centered on a piece of bead having a high concentration of binding sites and high when the bleach was centered on a void region. This bimodal distribution was not seen, supporting the homogeneous distribution assumption.

Secondary binding

The one site model assumes that the mobile macromolecule binds to a single type of site and that nonspecific binding or entrapment does not take place. While secondary interaction is difficult to quantify, a two site model is developed to demonstrate the relative importance of secondary interactions in the binding systems discussed in this paper. Secondary binding is taken into account by solving the diffusion equation with reversible binding to two competitive sites, a parallel reaction scheme. This two site model, developed in Appendix A, demonstrates that secondary interaction may be neglected if the affinity for the secondary site is weak or if the distribution of such sites is sparse. Appendix A demonstrates that the effect of

a racemic mixture of Mannose in the Concanavalin A/Mannose experiments is negligible.

Temperature increases

Mass transport and reaction parameters are temperature dependent. Local heating of the sample due to laser absorption by the sample and the fluorophore could alter these parameters. Laser beam characteristics and thermal effects for our system have been reviewed in reference 12. Welch et al. (25) proposed a model to account for heating due to absorption by the sample. As demonstrated in reference 12, sample absorption will lead to <0.04°C temperature rise in vitro (0.2 s bleaches). Simon et al. (26) calculated the temperature rise due to fluorophore absorption. Based upon these calculations, we expect less than a 1°C rise for the concentration of fluorophore in vitro. Both of these calculations are conservative because they assume that absorption is uniform with axial distance and neglect heat losses from the surface of the sample. Using the Stokes-Einstein Equation (23) and viscosities of water given in reference 27, a temperature increase of 2°C would increase the diffusion coefficient of Con A in water by 5%, a negligible amount compared with the standard deviation associated with measurement of this parameter. Successive bleaches are conducted at 5 min intervals to allow for data storage. This is sufficient time for the relaxation of any thermal gradient that does result from laser heating.

IN VIVO APPLICABILITY

One cannot a priori predict whether the time scale for a given binding interaction will be compatible with the time scales required by the FRAP technique. The mathematical model of diffusion with reversible binding made possible the assessment of the feasibility of using FRAP to measure the mass transport and reaction parameters for a given binding interaction. Using the one site model and assuming that the parameters of Dower et al. are correct, one sees in Fig. 3 that FRAP/GPD will be capable of reproducing these parameters as long as the concentration of antibody used in in vivo experiments can be held below 1×10^{-7} M. The requirement of low concentration of antibody could pose a problem because the binding species is the source of the fluorescence signal. As the concentration of fluorescent material (binding species) is decreased, the medium becomes increasingly more difficult to bleach and the signal-to-noise ratio in measuring the fluorescence intensity of the region is greatly decreased. The in vitro calibration using Con A did not present these problems due to a high concentration of Mannose in the sepharose matrix. The tumor, however,

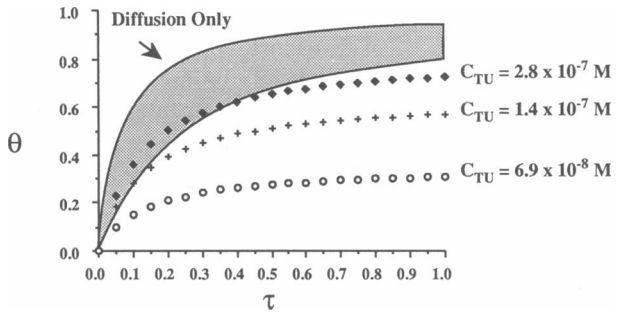

FIGURE 3 Recovery curves for a binding system as a function of the total concentration of binding species. The shaded region represents the area in which recovery is not significantly different from that of diffusion alone and binding parameters cannot be obtained. Kinetic parameters and concentration of binding sites are taken from Dower et al. (2); yielding $Da = 0.156$ and $\beta = 15.76$. Assuming Dower's parameters are correct, FRAP/GPD should be capable of reproducing them in vivo if the concentration of antibody in the interstitial space is kept below 1×10^{-7} M.

may have a very low concentration of binding sites which would require the use of a concentration of binding species lower than the 1×10^{-6} M FITC which has been found to be optimal in our FRAP studies. For this technique to have broad applicability, a more sensitive camera (e.g., ISIT or ICCD) or a fluorescent label with a more intense emission (e.g., BODIPY [28]) may have to be used.

The literature that exists representing in vitro studies of monoclonal antibody binding parameters (2, 29–37) demonstrate that due to the low concentration of binding sites, it may not always be possible to use the instantaneous binding model. In noninstantaneous regimes, Eqs. 12–15 must be repetitively solved numerically in any parameters estimation schemes to predict k_1, k_{-1}, Ag_0, and D. The task of parameter estimation and validation of the FRAP technique is the topic of ongoing research. Regardless of the binding model used, FRAP is capable of providing the pertinent binding parameters. Although the instantaneous model provides only D_{eff} from a single photobleach (or β if D is known) Baxter and Jain (manuscript submitted for publication) have recently established that if the interaction is instantaneous D_{eff} is all that is needed to predict macromolecular transport in vivo.

The models discussed thus far have assumed that no convective velocity fields exist in the region being monitored. Obviously this is not the case in vivo where the average interstitial fluid velocity (v) in the rabbit ear chamber preparation has been measured to be ~0.5 μm/s (5). Taking the diffusion coefficient for IgG (a molecule of interest for cancer detection and therapy) measured by FRAP to be 2.3×10^{-7} cm²/s (unpublished observations) and R_0 to be 4×10^{-3} cm, this translates to a Peclet

number ($Pe = vR_0/D$) of 0.87. When $Pe \gg 1$ convection is the dominant mode of transport, whereas when $Pe \ll 1$ diffusion is the dominant mode. By failing to account for the movement of the mobile macromolecule, the fluorescent intensity at the initial center point is overestimated (Fig. 4) leading to an overestimation of the diffusion coefficient. The effect of a convective field is most pronounced when no binding takes place because this represents the maximum flux of macromolecules into and out of the bleached region. Error analysis for the nonbinding case thus represents a worst case scenario because errors associated with convection in binding systems will be much smaller.

The dimensionless fluorescence intensity without binding as a function of dimensionless time and position is (12):

$$\theta(z, \tau) = 1 - \left(\frac{1}{1 + 8\tau}\right) \exp\left(\frac{-2z^2}{1 + 8\tau}\right). \quad (18)$$

Due to convection (plug flow), the position of the curve is displaced with time by an amount vt. The dimensionless displacement in time is $Pe\tau$. Accounting for the displacement of the curve due to convection, the dimensionless intensity at the initial center point of the Gaussian profile as a function of dimensionless time and Peclet number becomes:

$$\theta(z = 0, \tau, Pe) = 1 - \left(\frac{1}{1 + 8\tau}\right) \exp\left(\frac{-2(Pe\tau)^2}{1 + 8\tau}\right). \quad (19)$$

If convection is neglected (as done in this paper) the center point is expected to remain stationary and to have a dimensionless fluorescent intensity governed by Eq. 16.

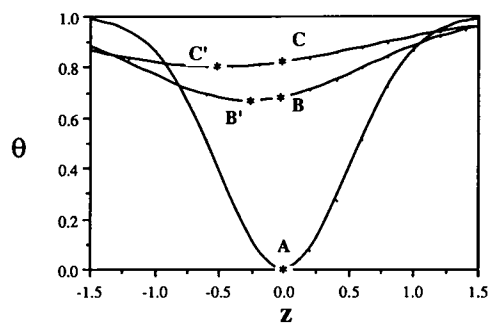

FIGURE 4 Overestimation of the center point fluorescence intensity associated with the neglection of a plug flow convection field. By failing to account for the plug flow convective field, here taken as $Pe = 1$ in the $-z$ direction, one slightly overestimates the fluorescent intensity at the "center point" by measuring A, B, C, at $\tau = 0$, 0.25, and 0.5, respectively instead of the true A, B', C'. This overestimation of the fluorescent intensity will lead to an overestimation of the diffusion coefficient.

Thus, by neglecting the convective field the center point intensity is overestimated by a factor of:

$$\% \text{ difference} = \frac{1 - \exp\left[\frac{-2(Pe\tau)^2}{1 + 8\tau}\right]}{8\tau} \times 100\%. \quad (20)$$

One sees in Fig. 5 that for the expected Peclet number and monitoring time, the error in measuring the center point intensity neglecting the plug flow convective field is ~2%. Even if the convective velocity were doubled, the error in measuring the center point intensity would be <10%. This overestimation of the center point intensities with time leads to an overestimation of the diffusion coefficient. If data is generated using Eq. 19 with $R_0 = 4 \times 10^{-3}$ cm and $D = 2.3 \times 10^{-7}$ cm^2/s for 12 s and this data is then fit to Eq. 16 to obtain the "measured" diffusion coefficient, one finds that neglecting the convective field leads to an overestimation of D by 2.6 and 11.3% for $Pe = 1$ and 2, respectively. This error is clearly insignificant compared with the ~30% standard deviation reported in measuring diffusion coefficients using GPD both in vivo and in vitro (5, 12).

The effect of convection will be less pronounced for binding systems. As demonstrated in Fig. 1, for FRAP/GPD to obtain parameters, the system must not be saturated. At this low concentration of binding species, <40% of the macromolecule will be mobile and will experience the moving profile seen in Fig. 4. Thus, for binding systems the overestimation of D (and subsequent underestimation of β) will be significantly less than the already acceptable 2.6% calculated above.

Because tracking the center point location is not required to obtain the parameters of interest, fitting the profile to a gaussian function at each time point, as was

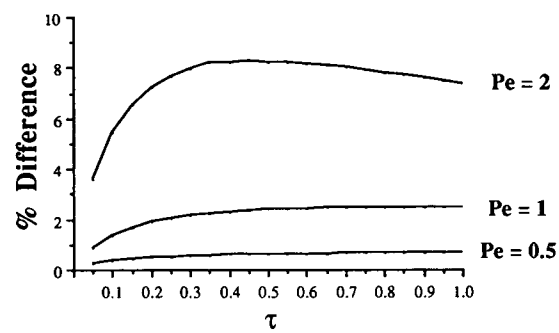

FIGURE 5 Percent overestimation of the "center point" dimensionless fluorescent concentration associated with neglecting the plug flow convective field as a function of dimensionless time and Peclet number. Note that for physiologically realistic Peclet numbers the percent error is ~2%.

done in the Con A calibration experiments, is unnecessary. One could make use of more of the available data by averaging the intensity over a small region centered about the bleached spot. Development, sensitivity, and feasibility of this method are given in Appendix B.

As discussed previously, the one site model assumes a uniform distribution of binding sites in the media through which the antibody is diffusing. This may not be realistic in all physiological situations. Chary and Jain (5) discuss how the application of FRAP in vivo may measure the diffusion coefficients of macromolecules in an "aqueous" rather than a "gel" like phase. They use this argument to describe why FRAP measures diffusion coefficients in vivo which are closer to the diffusion coefficient of the species in water than the lower in vivo diffusion coefficients measured using techniques (38) which monitor transport on a much longer time scale. If this is indeed the case, the binding sites must be in intimate contact with the "aqueous" phase for FRAP to detect the slower recovery due to binding in vivo. The uniformity of sites is in relation to the radius of the photobleached region. Cell surface antigens are confined to the surface of ~15-μm diam tumor cell, and not all the cells in the tumor mass may express a given antigen (39–41). Although any heterogeneity will be averaged over the 50-μm thickness of the rabbit ear chamber tissue preparation and ~90-μm diam of the bleached region, confinement to the cell surface as well as heterogeneous expression of the antigen may necessitate a more intricate model for certain antigens. The model presented in this paper best describes high molecular weight tumor associated antigens which are "shed" from the cell surface into the interstitial space such as Ferritin (42) or carcinoembryonic antigen (43). In vivo studies will first address the more simple mass transport problems of these shed antigens.

Secondary or nonspecific binding is difficult to quantify in vivo and one must report the effective reduction in diffusional rate due to binding. While such parameters may not represent the "true" kinetics of the monoclonal antibody/antigen interaction, they are useful for predicting monoclonal antibody distribution in vivo because they intrinsically account for nonspecific interaction. The two site model may be utilized to demonstrate the effects of nonspecific interactions and to place bounds as to when these interactions will alter the determination of primary interaction parameters.

As in the in vitro experiments, thermal effects may also be neglected in vivo. The temperature rise due to sample and fluorophore absorption are both <1°C for in vivo experiments. Again these figures are overestimations because the calculations do not account for convective heat loss due to blood flow.

Paucity of data

The one site model in a noninstantaneous regime requires the estimation of the four parameters D, k_1, k_{-1}, and Ag_0. Our current data acquisition system is able to discern a bleached spot for a system with no binding for only 12 s, and in that time is able to acquire data for only eight time points. Binding systems are discernable for a longer period of time due to their decreased effective diffusivity, but still may not yield enough data points to accurately estimate the four unknown parameters. The problem presented by the paucity of data may be overcome by reducing the number of unknown parameters that need to be estimated or by increasing the system's capability allowing more data to be acquired. The number of unknown parameters may be reduced by measuring the diffusion coefficient for the macromolecule independent of binding. This is most accurately accomplished by using an antibody of the same class, molecular weight, and charge as the monoclonal antibody under investigation which is not reactive with binding sites in the tumor. In many instances, the binding interaction will be instantaneous (as in the Con A/Mannose system) and will require the estimation of only the lumped binding parameter β. In most biological binding interactions, the key component determining the magnitude of the Damkoehler number (which determines if the interaction is instantaneous) will be the concentration of binding sites. Work by Guadagni et al. (44, 45) has demonstrated that for some tumor associated antigens it is possible to dramatically increase the concentration of binding sites through the administration of interferon. It may thus be possible using interferon to both render an interaction instantaneous which was not so before and simultaneously allow for the use of a higher concentration of binding species. The capability of the data acquisition system may be increased through improved technology or alternative measurement techniques. Improved data acquisition boards may triple the rate of data acquisition thereby tripling the amount of data. Improved objectives and more sensitive cameras may be capable of discerning the bleached region for longer periods of time, further increasing the amount of available data. In this paper, the center point position and concentration were determined by fitting the intensity data to a gaussian function. This required the acquisition of a large number of pixels at each time point and hence a longer data acquisition time. As demonstrated earlier, fitting to a gaussian profile and tracking the center point position is unnecessary. One may "fix" the center point or average the intensity over a small region with minimal error associated in measuring the diffusion coefficient and with fewer pixels acquired at each time point. This will

dramatically increase the data acquisition rate, providing adequate data for parameter estimation.

Through the methods developed in this paper, FRAP is capable of accurately measuring the pertinent mass transport and binding parameters from a single photobleach. In conjunction with the rabbit ear chamber or similar tissue preparation, this will allow the first quantification of these parameters in vivo and will yield the most clinically relevant parameters to date for use in improving the delivery of therapeutic agents to their target tissue. Unlike previous methods to measure these parameters, this method is capable of being conducted in vivo, does not intrinsically alter the system of interest, and does not require a priori knowledge or variation of system parameters.

APPENDIX A

Two site model

Theoretical development of the two site binding model, like the one site model, assumes a uniform distribution of binding sites, an immobile bound complex, and no convective field. The diffusion equation with reversible binding to two competing sites is:

$$C_1 \begin{array}{l} + Ag_1 \underset{k_{-1}}{\overset{k_1}{\rightleftharpoons}} C_2 \\ + Ag_2 \underset{k_{-2}}{\overset{k_2}{\rightleftharpoons}} C_3 \end{array} \tag{A1}$$

$$\frac{\partial C_{1i}}{\partial t} = D\nabla^2 C_{1i} - k_1 C_{1i} Ag_1 + k_{-1} C_{2i} - k_2 C_{1i} Ag_2 + k_{-2} C_{3i} \tag{A2}$$

$$\frac{\partial C_{2i}}{\partial t} = k_1 C_{1i} Ag_1 - k_{-1} C_{2i} \tag{A3}$$

$$\frac{\partial C_{3i}}{\partial t} = k_2 C_{1i} Ag_2 - k_{-2} C_{3i}. \tag{A4}$$

These equations are written for fluorescently active ($i = a$) and bleached ($i = b$) molecules. Ag_0 is the total concentration of binding sites. xAg_0 is the concentration of "primary" sites which lead to the C_{2i} bound complex, whereas $(1 - x)Ag_0$ is the concentration of secondary sites leading to C_{3i}. The Laplacian operator and the initial condition on C_{Ta} ($C_{Ta} = C_{1a} + C_{2a} + C_{3a}$) are identical to those in the one site model. The initial conditions for the individual components are defined by the four equilibrium conditions that may be written in a similar fashion as Eqs. 6 and 7. These equilibrium conditions as well as the initial condition for C_{Ta} and the definition of C_{Tb} represent six nonlinear algebraic equations for the six components and may be solved numerically. The boundary conditions for the components are defined in a similar manner as the one site model Eq. 8.

The differential equations were made dimensionless by introducing the following groups:

$$\theta_{Ta} = \theta_{1a} + \theta_{2a} + \theta_{3a} = \frac{C_{Ta} - C_{TB}}{C_{TU} - C_{TB}} \tag{A5}$$

$$\theta_{1a} = \frac{C_{1a}}{C_{TU} - C_{TB}}$$

$$\theta_{2a} = \frac{C_{2a}}{C_{TU} - C_{TB}} \qquad \theta_{3a} = \frac{C_{3a} - C_{TB}}{C_{TU} - C_{TB}} \tag{A6}$$

$$\theta_{TB} = 1 - \theta_{Ta} = \theta_{1b} + \theta_{2b} + \theta_{3b} = \frac{C_{Tb}}{C_{TU} - C_{TB}} \tag{A7}$$

$$\theta_{1b} = \frac{C_{1b}}{C_{TU} - C_{TB}}$$

$$\theta_{2b} = \frac{C_{2b}}{C_{TU} - C_{TB}} \qquad \theta_{3b} = \frac{C_{3b}}{C_{TU} - C_{TB}} \tag{A8}$$

$$z = \frac{r}{R_0} \qquad \tau = \frac{Dt}{R_0^2} \qquad \gamma = \frac{C_{TB}}{C_{TU} - C_{TB}} \tag{A9}$$

$$Da_1 = \frac{R_0^2 k_1 x Ag_0}{D} \qquad \beta_1 = \frac{k_1 x Ag_0}{k_{-1}} \qquad \alpha_1 = \frac{C_{TB}}{x Ag_0} \tag{A10}$$

$$Da_2 = \frac{R_0^2 k_2 (1 - x) Ag_0}{D}$$

$$\beta_2 = \frac{k_2 (1 - x) Ag_0}{k_{-2}} \qquad \alpha_2 = \frac{C_{TB}}{(1 - x) Ag_0}. \tag{A11}$$

The equations describing the fluorescent recovery after photobleaching become:

$$\frac{\partial \theta_{1a}}{\partial \tau} = \frac{1}{z}\frac{\partial}{\partial z}\left(z \frac{\partial \theta_{1a}}{\partial z}\right) - Da_1 \left(\theta_{1a}\left\{1 - \alpha_1\left[\frac{1}{\gamma}(\theta_{2a} + \theta_{2b})\right]\right\} - \frac{\theta_{2a}}{\beta_1}\right) - Da_2 \left(\theta_{1a}\left\{1 - \alpha_2\left[\frac{1}{\gamma}(\theta_{3a} + \theta_{3b}) + 1\right]\right\} - \frac{(\theta_{3a} + \gamma)}{\beta_2}\right) \tag{A12}$$

$$\frac{\partial \theta_{1b}}{\partial \tau} = \frac{1}{z}\frac{\partial}{\partial z}\left(z \frac{\partial \theta_{1b}}{\partial z}\right) - Da_1 \left(\theta_{1b}\left\{1 - \alpha_1\left[\frac{1}{\gamma}(\theta_{2a} + \theta_{2b})\right]\right\} - \frac{\theta_{2b}}{\beta_1}\right) - Da_2 \left(\theta_{1b}\left\{1 - \alpha_2\left[\frac{1}{\gamma}(\theta_{3a} + \theta_{3b}) + 1\right]\right\} - \frac{(\theta_{3b})}{\beta_2}\right) \tag{A13}$$

$$\frac{\partial \theta_{2a}}{\partial \tau} = Da_1 \left(\theta_{1a}\left\{1 - \alpha_1\left[\frac{1}{\gamma}(\theta_{2a} + \theta_{2b})\right]\right\} - \frac{(\theta_{2a})}{\beta_1}\right) \tag{A14}$$

$$\frac{\partial \theta_{2b}}{\partial \tau} = Da_1 \left(\theta_{1b}\left\{1 - \alpha_1\left[\frac{1}{\gamma}(\theta_{2a} + \theta_{2b})\right]\right\} - \frac{(\theta_{2b})}{\beta_1}\right) \tag{A15}$$

$$\frac{\partial \theta_{3a}}{\partial \tau} = Da_2 \left(\theta_{1a}\left\{1 - \alpha_2 \cdot \left[\frac{1}{\gamma}(\theta_{3a} + \theta_{3b}) + 1\right]\right\} - \frac{(\theta_{3a} + \gamma)}{\beta_2}\right) \tag{A16}$$

$$\frac{\partial \theta_{3b}}{\partial \tau} = Da_2 \left(\theta_{1b}\left\{1 - \alpha_2\left[\frac{1}{\gamma}(\theta_{3a} + \theta_{3b}) + 1\right]\right\} - \frac{\theta_{3b}}{\beta_2}\right). \tag{A17}$$

All terms are defined as in the one site model with the additional subscripts 1 for primary and 2 for secondary interaction. The six coupled nonlinear partial differential equations were solved numerically.

The sugar D-Mannose when in solution, exists in two different optical conformations. The β conformation comprises 32.6% of the population (46) and has a dissociation constant which is an order of magnitude

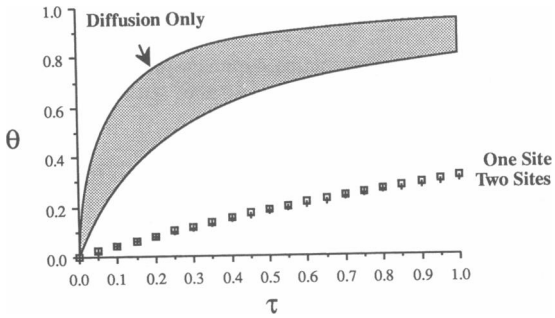

FIGURE 6 Effect of a racemic mixture of Mannose binding sites on Con A recovery curve. The shaded region represents the area in which recovery is not significantly different from that of diffusion alone and binding parameters cannot be obtained. Parameters used for this simulation are: $Da_1 = 1{,}849$, $Da_2 = 894$, $\beta_1 = 16.85$, $\beta_2 = 0.96$, $\alpha_1 = 0.011$, $\alpha_2 = 0.002$, $\gamma = 3$. Secondary binding to β Mannose does not alter the recovery curve for Con A's binding to Mannose in product M6400.

higher than that of α D-Mannose (17). As seen in Fig. 6, if the immobilized Mannose binding sites in product M6400 are in a racemic mixture, the effect of secondary binding to the β Mannose is negligible when compared with one site binding to the α sugar when Ag_0 in the one site model is reduced 32.6%.

APPENDIX B

Window averaging technique

The window averaging technique is analogous to the photomultiplier/aperture technique used in reference 47. The use of video digitization, however, allows for a more sensitive placement of the monitoring region than an aperture. Development of the window averaging technique proceeds along a similar line as the analysis of the no convection assumption. The window size is first optimized using a nonbinding model. Again the nonbinding case represents a worst case scenario because convection without binding yields the largest flux of mobile macromolecule and the largest associated error. Integration of the numerical solutions obtained for the GPD method then provides sensitivity and feasibility analysis for the window averaging technique.

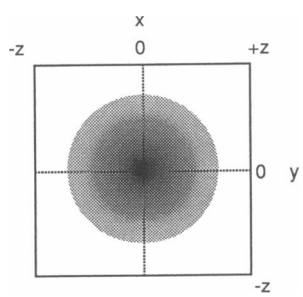

FIGURE 7 The fluorescence intensity is integrated over a rectangular region to obtain the average intensity in this region.

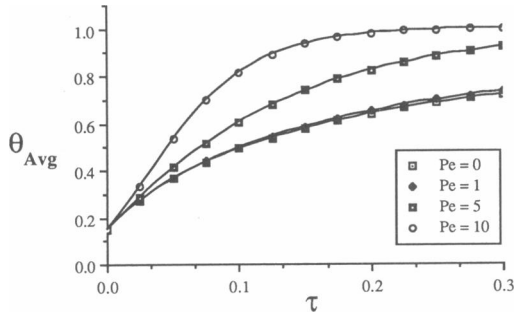

FIGURE 8 Dimensionless average concentration as a function of dimensionless time and Peclet number for dimensionless region size $u = 0.5$. Negligible error is incurred by neglecting convection for physiologically realistic Peclet numbers.

The total fluorescence intensity as a function of space and time following a gaussian photobleach (no binding) is (12):

$$C(x, y, t) = C_{TU} - (C_{TU} - C_{TB})\left\{\left[1 - \frac{\left(\frac{8Dt}{R_0^2}\right)}{1 + \left(\frac{8Dt}{R_0^2}\right)}\right]\exp\left[\frac{-2(x^2 + y^2)}{R_0^2 + 8Dt}\right]\right\}, \quad \text{(B1)}$$

where terms are defined as in the GPD development. The DT IRIS acquisition board allows for only rectangular monitoring regions so this analysis integrates over a square window (Fig. 7). If one wishes to use a circular aperture, one integrates in cylindrical coordinates and will obtain a simpler mathematical expression.

The average intensity in a square window of area $4z^2$ is:

$$C_{Avg} = \frac{1}{4z^2}\int_{-z}^{z}\int_{-z}^{z} C\, dx\, dy. \quad \text{(B2)}$$

Performing this integration and making the equation dimensionless

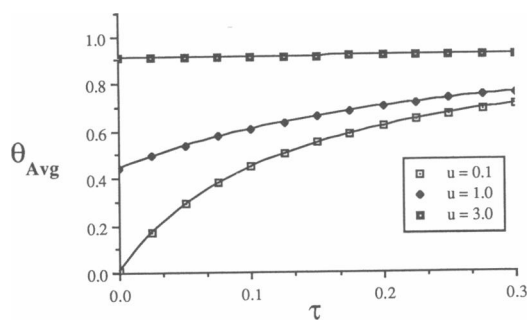

FIGURE 9 Dimensionless average concentration as a function of dimensionless time and region size. As the region size increases, recovery occurs over a smaller range of dimensionless concentration, decreasing the system's resolution.

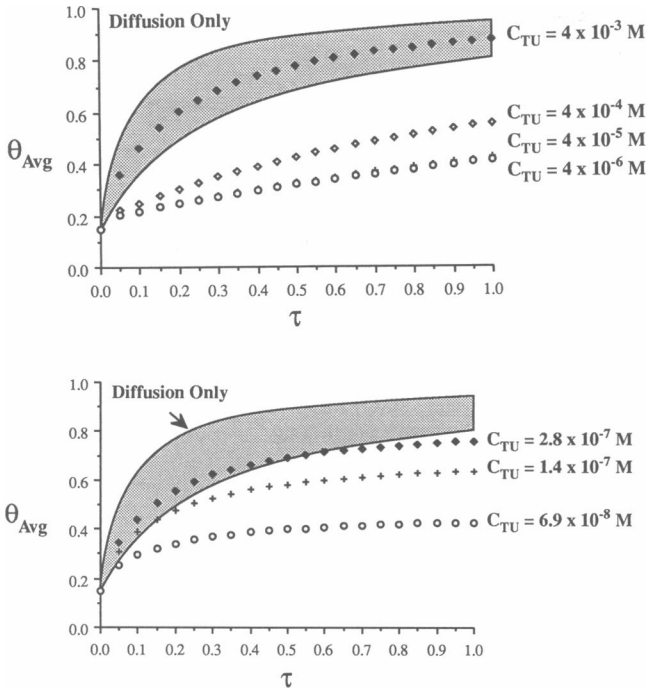

FIGURE 10 Sensitivity and feasibility graphs for the window averaging technique. The shaded region represents the area in which recovery is not significantly different from that of diffusion alone and binding parameters cannot be obtained. Simulations were run with $u = 0.5$ and the same parameters as used in Figs. 1 and 3, respectively. Conclusions are analogous.

yields:

$$\theta_{Avg} = \frac{C_{Avg} - C_{TB}}{C_{TU} - C_{TB}} = 1 - \frac{\pi}{4u^2} erf^2\left(\frac{u}{\sqrt{1 + 8\tau}}\right) \quad \text{(B3)}$$

$$u = \frac{\sqrt{2}z}{R_0}, \quad \text{(B4)}$$

u being the dimensionless size of the window.

In the presence of convection, the x and y terms in Eq. B1 must be replaced by $x + v_x t$ and $y + v_y t$, respectively, where v_x and v_y are the convective velocities in the x and y directions. The dimensionless average concentration as a function of dimensionless time, region size, and Peclet number becomes:

$$\theta_{Avg} = 1 - \frac{\pi}{16u^2}\left[erf\left(\frac{u + \sqrt{2\tau}Pe_x}{\sqrt{1 + 8\tau}}\right) + erf\left(\frac{u - \sqrt{2\tau}Pe_x}{\sqrt{1 + 8\tau}}\right)\right] \times \left[erf\left(\frac{u + \sqrt{2\tau}Pe_y}{\sqrt{1 + 8\tau}}\right) + erf\left(\frac{u - \sqrt{2\tau}Pe_y}{\sqrt{1 + 8\tau}}\right)\right]. \quad \text{(B5)}$$

The window averaging technique presents an interesting optimization problem. One wishes to use a large window size so that the system is robust and the convective velocity field does not "push" the bleached spot out of the monitoring region (Fig. 8). However, one wishes to use a small enough monitoring region to have recovery over a large range of dimensionless concentration (Fig. 9), increasing the system's resolution. The window size used in the simulations presented here was arbitrarily chosen as the smallest window size which would have an error due to the neglection of convection of <2% for $Pe = 1$. The average intensity in binding simulations was calculated by integrating the numerical solutions to Eq. 12–15. Fig. 10, *a* and *b* show sensitivity and in vivo feasibility graphs analogous to Figs. 1 and 3.

The authors wish to thank R. Martin, L. Baxter, Dr. R. Stock, Dr. H. Toor, Dr. D. Axelrod, and Dr. E. Ko for their valuable suggestions and assistance.

This work was supported by a grant from the National Institutes of Health (CA-36902). E. N. Kaufman is a recipient of a W. M. Keck Predoctoral Fellowship.

Received for publication 4 December 1989 and in final form 16 May 1990.

REFERENCES

1. Jain, R. 1989. Delivery of novel therapeutic agents in tumors: physiological barriers and strategies. *J. Natl. Cancer Inst.* 81:570–576.
2. Dower, S., K. Ozato, and D. Segal. 1984. The interaction of monoclonal antibodies with MHC class I antigens on mouse spleen cells I. Analysis of the mechanism of binding. *J. Immunol.* 132:751–758.
3. McFadden, R., and C. Kwok. 1988. Mathematical model of simultaneous diffusion and binding of antitumor antibodies in multicellular human tumor spheroids. *Cancer Res.* 48:4032–4037.
4. Sandison, J. 1924. A new method for microscopy study of living growing tissues by the introduction of a transparent chamber in the rabbit's ear. *Anat. Rec.* 28:281–287.
5. Chary, S., and R. Jain. 1989. Direct measurement of interstitial convection and diffusion of albumin in normal and neoplastic tissues by fluorescence photobleaching. *Proc. Natl. Acad. Sci. USA.* 86:5385–5389.
6. Burghardt, T., and D. Axelrod. 1981. Total internal reflection/fluorescence photobleaching recovery study of serum albumin adsorption dynamics. *Biophys. J.* 33:455–468.
7. Thompson, N., and D. Axelrod. 1983. Immunoglobulin surface-binding kinetics studied by total internal reflection with fluorescence correlation spectroscopy. *Biophys. J.* 43:103–114.
8. Axelrod, D., R. Fulbright, and E. Hellen. 1986. Adsorption kinetics on biological membranes: measurement by total internal reflection fluorescence. *In* Applications of Fluorescence in the Biomedical Sciences. D. L. Taylor, A. S. Waggoner, R. F. Murphy, F. Lanni, and R. R. Birge, editors. Alan R. Liss, Inc., New York. 461–476.
9. Elson, E., and J. Reidler. 1979. Analysis of cell surface interactions by measurements of lateral mobility. *J. Supramol. Struct.* 12:481–489.
10. Koppel, D. 1981. Association Dynamics and Lateral Transport in Biological Membranes. *J. Supramol. Struct.* 17:61–67.
11. Chary, S., and R. Jain. 1987. Analysis of diffusive and convective recovery of fluorescence after photobleaching. Effect of uniform flow field. *Chem. Eng. Comm.* 55:235–249.
12. Jain, R., R. Stock, S. Chary, and M. Rueter. 1990. Convection and diffusion measurements using fluorescence recovery after photobleaching and video image analysis: *in vitro* calibration and assessment. *Microvasc. Res.* 39:77–93.

13. Kwok, C., and S. Cole. 1988. Uptake kinetics of monoclonal antibodies by human malignant melanoma multicell spheroids. *Cancer Res.* 48:1856–1863.

14. Gray, R., and R. Glew. 1973. The kinetics of carbohydrate binding to concanavalin A. *J. Biol. Chem.* 248:7547–7551.

15. Crank, J. 1975. The Mathematics of Diffusion. Clarendon Press, Oxford. 326–327.

16. Clegg, R., F. Loontiens, and T. Jovin. 1977. Binding of 4-Methylumbelliferyl α-D-Mannopyranoside to dimeric concanavalin A: fluorescence temperature-jump relaxation study. *Biochemistry.* 16: 167–175.

17. Farina, R., and R. Wilkins. 1980. Kinetics of interaction of some α- and β-D-Monosaccharides with concanavalin A. *Biochim. Biophys. Acta.* 631:428–438.

18. Loontiens, F., R. Clegg, and T. Jovin. 1977. Binding of 4-Methylubelliferyl α-D-Mannopyranoside to tetrameric and unmodified or derivatized concanavalin A: equilibrium studies. *Biochemistry.* 16:159–166.

19. Gunther, G., J. Wang, I. Yahara, B. Cunningham, and G. Edelman. 1973. Concanavalin A derivatives with altered biological activities. *Proc. Natl. Acad. Sci. USA.* 70:1012–1016.

20. Nugent, L., and R. Jain. 1984. Plasma pharmacokinetics and interstitial diffusion of macromolecules in a capillary bed. *Amer. J. Physiol.* H129–H137.

21. Bard, Y. 1974. Nonlinear Parameter Estimation. Academic Press, New York.

22. Liener, I. 1976. Isolation and properties of concanavalin A. *In* Concanavalin A as a Tool. H. Bittiger and H. Schnebli, editors. John Wiley & Sons Ltd., London. 17–31.

23. Cussler, E. 1986. Diffusion: Mass Transfer in Fluid Systems. Cambridge University Press, Cambridge. 119.

24. Becker, J., B. Cunningham, G. Reeke, J. Wang, and G. Edelman. 1976. The molecular structure of concanavalin A. *In* Concanavalin A as a Tool. H. Bittiger and H. Schnebli, editors. John Wiley & Sons Ltd., London. 33–54.

25. Welch, A., E. Wissler, and L. Priebe. 1980. Significance of blood flow in calculations of temperature in laser irradiated tissue. *IEEE (Inst. Electr. Electron. Eng.) Trans. Biomed. Eng.* 27:164–166.

26. Simon, J., A. Gough, E. Urbanik, F. Wang, F. Lanni, B. Ware, and D. Taylor. 1988. Analysis of rhodamine and fluorescein-labeled F-actin diffusion in vitro by fluorescence photobleaching recovery. *Biophys. J.* 54:801–815.

27. Weast, R. 1976. CRC Handbook of Chemistry and Physics. CRC Press, Inc., Cleveland. F-51.

28. Molecular Probes, Inc. 1989. *Bioprobes.* (Advertisement of Molecular Probes, Inc., Eugene, OR).

29. Blasberg, R., H. Nakagawa, M. Bourdon, D. Groothuis, C. Patlak, and D. Bigner. 1987. Regional localization of a glioma-associated antigen defined by monoclonal antibody 81C6 *in vivo:* kinetics and implications for diagnosis and therapy. *Cancer Res.* 47:4432–4443.

30. Brown, B., G. Davis, J. Saltzgaber-Muller, P. Simon, M. Ho, P. Shaw, B. Stone, H. Sands, and G. Moore. 1987. Tumor-specific genetically engineered murine/human chimeric monoclonal antibody. *Cancer Res.* 47:3577–3583.

31. Kalofonos, H., G. Rowlinson, and A. Epenetos. 1990. Enhancement of monoclonal antibody uptake in human colon xenografts following irradiation. *Cancer Res.* 50:159–163.

32. Sheer, D., J. Schlom, and H. Cooper. 1988. Purification and composition of human tumor-associated glycoprotein (TAG-72) defined by monoclonal antibodies CC49 and B72.3. *Cancer Res.* 48:6811–6818.

33. Steller, M., R. Parker, D. Covell, O. Holton, A. Kennan, S. Seiber, and J. Weinstein. 1986. Optimization of monoclonal antibody delivery via the lymphatics: the dose dependance. *Cancer Res.* 46:1830–1834.

34. Beatty, J., B. Beatty, and W. Vlahos. 1987. Measurement of monoclonal antibody affinity by non-competitive enzyme immunoassay. *J. Immunol. Methods.* 100:173–179.

35. Douillard, J., J. Laborda, C. Burg, J. Ridge, I. Levenbook, H. Blottiere, S. Ami, and T. Hoffman. 1989. Monoclonal antibodies to a rat colon carcinoma: model for monoclonal antibody therapy of solid tumors. *Cancer Res.* 49:687–692.

36. Molinolo, A., J. Simpson, A. Thor, and J. Schlom. 1990. Enhanced tumor binding using immunohistochemical analysis by second generation anti-tumor-associated glycoprotein 72 monoclonal antibodies *versus* monoclonal antibody B72.3 in human tissue. *Cancer Res.* 50:1291–1298.

37. Ong, G., and M. Mattes. 1989. Penetration and binding of antibodies in experimental human solid tumors grown in mice. *Cancer Res.* 49:4264–4273.

38. Nugent, L., and R. Jain. 1984. Extravascular diffusion in normal and neoplastic tissue. *Cancer Res.* 44:238–244.

39. Epenetos, A. A., D. Snook, H. Durbin, P. M. Johnson, and J. T. Papadimitrio. 1986. Limitations of radiolabeled monoclonal antibodies for localization of human neoplasms. *Cancer Res.* 46:3183–3191.

40. Dykes, P., A. Bradwell, C. Chapman, and A. Vaughan. 1987. Radioimmunotherapy of cancer: clinical studies and limiting factors. *Cancer Treat. Rev.* 14:87–106.

41. Sutherland, R., F. Buchegger, M. Schreyer, A. Vacca, and J. Mach. 1987. Penetration and binding of radiolabeled anti-carcinoembryonic antigen monoclonal antibodies and their antigen binding fragments in human colon multicellular tumor spheroids. *Cancer Res.* 47:1627–1633.

42. Order, S. 1977. Antigens, immunoglobulins, and immunity during the course of breast cancer. *Prog. Clin. Biol. Res.* 12:119–130.

43. Moshakis, V., M. Ormerod, J. Westwood, S. Imrie, and A. Neville. 1982. The site of binding of anti-CEA antibodies to tumor CEA in vivo: an immunocytochemical and autoradiographic approach. *Br. J. Cancer.* 48:18–21.

44. Guadagni, F., J. Schlom, S. Pothen, S. Peestka, and J. Greiner. 1988. Parameters involved in the enhancement of monoclonal antibody targeting in vivo with recombinant interferon. *Cancer Immunol. Immunother.* 26:222–230.

45. Guadagni, F., J. Schlom, W. Johnston, C. Szpak, D. Goldstein, R. Smalley, J. Simpson, E. Borden, S. Pestka, and J. Greiner. 1989. Selective interferon-induced enhancement of tumor-associated antigens on a spectrum of freshly isolated human adenocarcinoma cells. *J. Natl. Cancer Inst.* 81:502–512.

46. Streitwieser, A., and C. Heathcock. 1981. Introduction to Organic Chemistry. Macmillan Publishing Co. Inc., New York. 934.

47. Thompson, N., T. Burghardt, and D. Axelrod. 1981. Measuring surface dynamics of biomolecules by total internal reflection fluorescence with photobleaching recovery or correlation spectroscopy. *Biophys. J.* 33:435–454.

48. Hecht, E., and A. Zajac. 1979. Optics. Addison-Wesley Publishing Co., Reading, MA.

49. Axelrod, D., D. Koppel, J. Schlessinger, E. Elson, and W. Webb. 1976. Mobility measurement by analysis of fluorescence photobleaching recovery kinetics. *Biophys. J.* 16:1055–1069.